Modeling of Kinetics of Air Entrainment in Water Produced by Vertically Falling Water Flow

Adelė VAIDELIENĖ [2] [*], Arvaidas GALDIKAS [1, 4], Paulius TERVYDIS [3]

[1] *Department of Physics, Kaunas University of Technology, Studentų 50, LT-51368 Kaunas, Lithuania*

[2] *Lithuanian Energy Institute, Breslaujos 3, LT-44403 Kaunas, Lithuania*

[3] *Department of Telecommunications, Kaunas University of Technology, Studentų 50, LT-51368 Kaunas, Lithuania*

[4] *Department Physics, Mathematics and Biophysics, Lithuanian University of Health Sciences, Eivenių 4, LT-50166, Kaunas, Lithuania*

This study analyzes the process of air entrainment in water caused by vertically falling water flow in the free water surface. The new kinetic model of air entrainment in water was developed. This model includes the process of air entrapment, as well as air removal, water sputtering and resorption. For the experimental part of this study a new method based on digital image processing was developed. Theoretical and experimental methods were used for determining air concentration and its distribution in water below the air-water interface. A new presented mathematical model of air entrainment process allows determining of air bubbles and water droplets concentrations distribution. The obtained theoretical and experimental results were in good agreement.

Keywords: vertical water flow, entrainment, rise, sputtering, concentration distribution, air, water.

1. INTRODUCTION

A vertically falling water jet impingement in a quiescent water vessel creates an air entrainment in water. The air entrapment in the water also appears when the water moves through wears of hydropower stations or through river rifts. Waves in large open water bodies such as reservoirs, lakes, seas and oceans also stimulate air entrainment. The air entrainment in the water is an integrate part of the water aeration process, that on its own turn leads to the water purification.

The entrainment of gases in liquid trough multiphase flows is widely used in various fields of science, industry and environmental engineering. In chemistry bubbly flows are used to improve liquids mixing processes [1 – 5]. The air entrainment in the water by plunging the water jet has a potential application in many technological processes, for example, in the waste water treatment [6 – 10]. The water aeration processes are important tools of environment engineering because they highly influence the process of self-purification in rivers and other open reservoirs of the water [11 – 16]. One of the important factors of liquid aeration is a mixture of air bubbles and water droplets. This phenomenon was investigated by Chanson, Hoque, Karwa et. al. [17 – 19].

Understanding of mechanism of the air bubbles and the water droplets mixing produced by the water jet impinging on a free water surface has its practical importance, also, for the effective modelling of heat and mass transfer processes because in both cases the problem deals with two phase systems [20 – 24].

The goal of this paper is to develop mathematical model that allows a determination and prediction of air bubbles and water droplets concentration and its distribution in the zone of "white water" and verify it experimentally.

2. KINETIC MODEL

Due to the vertical water flow falling into the free water surface the water mixing occurs in the air-water interface. As a result of this, mixing air is entrained in the deeper water layers. The air-water mixture exists not only under the air-water interface but also above this interface because under water surface the air-water mixture blows up, the air bubbles rise up and are removed from the water. The falling water can also knock out the water sprays that can evaporate or fall down on the water surface. The fallen sprays can knock out new water sprays or be absorbed by the water. For description of all these processes we have developed a mathematical model. The model has significant relevance to development and improvement of aeration process and can be used for practical purposes. The proposed theoretical model is one-dimensional entrapment of air at the free-falling jet.

All air entrainment zone we split up into K monolayers that can be filled with air, water or sum of them. Normalized filling function of j-th monolayer was introduced:

$$\varphi^{(j)} = \varphi_1^{(j)} + \varphi_2^{(j)} = 1, \text{ when } j = 1, 2, ..., K-1, K, K+1, \tag{1}$$

Where $\varphi_1^{(j)}$ and $\varphi_2^{(j)}$ are functions of the monolayer filling with water and air respectively. Filling of K-th monolayer with air or water is continually varying. Rate of this functions $\varphi_1^{(j)}$, $\varphi_2^{(j)}$ can be described as a sum of equations of entrainment, removal, sputtering, evaporation and resorption rate:

---

[*]Corresponding author. Tel.: +370-37-401966, fax: +370-37-351271.
E-mail address: *avaidel@mail.lei.lt* (A. Vaidelienė)

$$\begin{cases} \dfrac{d\varphi_i^{(j)}}{dt} = \left(\dfrac{d\varphi_i^{(j)}}{dt}\right)_{en} + \left(\dfrac{d\varphi_i^{(j)}}{dt}\right)_{el} + \left(\dfrac{d\varphi_i^{(j)}}{dt}\right)_{sp+ev} + \left(\dfrac{d\varphi_i^{(j)}}{dt}\right)_{resorb}, \; j=1,2,...,K,K+1, \\ i=1,2 \end{cases} \quad (2)$$

where subscripts *en* – entrainment, *el* – elimination, *sp+ev* – sputtering and evaporation, *resorb* – resorption.

Solutions of Eq. (2) are concentrations of air bubbles and water droplets due to turbulent flows produced by free vertical water jet hitting the free water surface.

Let us discuss each process separately.

2.1. Entrainment and removal

Assuming that in *K*-th monolayer the rate of air entrainment in the water is proportional to the falling water flow $i_H^{(K)}$ the rate of filling functions can be written as follow:

$$\begin{cases} \left(\dfrac{d\varphi_1^{(j)}}{dt}\right)_{en} = i_H^{(j)} \cdot \beta \\ \left(\dfrac{d\varphi_2^{(j)}}{dt}\right)_{en} = i_H^{(j)} \cdot Fr_1 \cdot \beta \end{cases} \quad j=1,2,...,K-1,K,K+1; \quad (3)$$

$$Fr_1 = \dfrac{v_1}{\sqrt{g\,d_1}}, \quad (4)$$

where Fr_1 – dimensionless impingement Froude number [26]. Usually, the air entrapped into depth is distributed according to Gaussian law [25]:

$$i_H^{(j)} = i_0 \cdot \exp\left[-\dfrac{1}{2}\left(\dfrac{K \cdot dd - R_p}{\Delta R_p}\right)^2 \right], \quad (4a)$$

where i_0 (s^{-1}) is the total water jet flux, dd (m) is the mean value of thickness of the monolayer, R_p (m) is the average penetration of depth of air and ΔR_p (m) is the standard deviation, β – dimensionless coefficient, which is equal to the probability of finding entrapped air or water in the varied monolayer, v_1 – water flow velocity in incident flux zone (m/s), g – acceleration due to gravity (m/s^2), d_1 – is the jet impact diameter (m).

The maximum depth of the air entrainment into the water can be calculated as follow [27]:

$$z_p = \dfrac{1.2 \cdot v_1^{0.77} \cdot d_0^{0.625}}{k_L \cdot h^{0.094}}, \quad (4b),$$

$$R_p = z_p / 2,$$

where z_p is the maximum penetration depth of air, d_0 is the jet nozzle diameter, h is the distance from nozzle tip to the water surface, $k_L = 1.0$ is the overall mass transfer coefficient (s^{-1}).

Solving equation (3), we have assumed that the top layer filled with water monolayer is *m*-th, and the *K*-th – monolayer is the deepest. Accordingly, we have chosen that the following boundary conditions when $t = 0$:

$\varphi_1^{(j)}(0)=1$, if $m \le j \le K$ $\varphi_1^{(j)}(0)=0$, if $1 \le j < m$ and

$\varphi_2^{(j)}(0)=0$, if $m \le j \le K$ $\varphi_2^{(j)}(0)=1$, if $1 \le j < m$; $\dot{\varphi}_1^{(K)} = \dot{\varphi}_1^{(K+1)}$.

From equation (3) it is seen that $\varphi_1^{(j)}$, $\varphi_2^{(j)}$ grows infinitely during the entrapment process. Therefore, in order to keep the condition $\varphi^{(j)} = 1$, it is necessary to perform renormalization of monolayers. The *K-th* layer's

air and water overall total amount, which exceeds one (>1) i.e. $\varphi*^{(j)} = \varphi^{(j)} - 1$ is displaced into the $(K-1)$ monolayer. Fractions of the air $f_2^{(j)}$ and water $f_1^{(j)}$ taking place in the *K*-th monolayer can be calculated as follows:

$$f_2^{(j)} = \varphi_2^{(j)} / \left(\varphi_1^{(j)} + \varphi_2^{(j)}\right); \quad (5)$$

$$f_1^{(j)} = \varphi_1^{(j)} / \left(\varphi_1^{(j)} + \varphi_2^{(j)}\right). \quad (6)$$

Total amount of the air and water displaced from *K*-th layer into $(K-1)$ layer must have the same ratio that it had in *K*-layer. Displaced parts of the air $\varphi*_2^{(K)}$ and water $\varphi*_1^{(K)}$ can be expressed with this equation:

$$\begin{cases} \varphi*_2^{(j)} = \begin{cases} f_2^{(j)} \cdot \left(\left(\varphi_1^{(j)}+\varphi_2^{(j)}\right)-1\right), \; if \left(\varphi_1^{(j)}+\varphi_2^{(j)}\right)>1 \\ 0, \quad if \left(\varphi_1^{(j)}+\varphi_2^{(j)}\right)\le 1 \end{cases} \\ \varphi*_1^{(j)} = \begin{cases} f_1^{(j)} \cdot \left(\left(\varphi_1^{(j)}+\varphi_2^{(j)}\right)-1\right), \; if \left(\varphi_1^{(j)}+\varphi_2^{(j)}\right)>1 \\ 0, \; if \left(\varphi_1^{(j)}+\varphi_2^{(j)}\right)\le 1 \end{cases} \end{cases} j=1,2,...K-1,K. \quad (7)$$

Evaluating equation (7), filling of the monolayer $(K-1)$ with the air and water can be recalculated as follow:

$$\begin{cases} \varphi_2^{(j-1)} = \left(\varphi_2^{(j-1)}\right) + \varphi*_2^{(j)} \\ \varphi_1^{(j-1)} = \left(\varphi_1^{(j-1)}\right) + \varphi*_1^{(j)} \end{cases} j=1,2,...,K-1,K,K+1. \quad (8)$$

The air bubbles entrained in the water under acting of Archimedes force raises from the deeper layers to the water surface. Part of the bubbles joins upper monolayers bubbles and increases in volume. This process is analogous to process of liquids boiling where the air bubbles increases going up to the water surface. Consequently, the ensuing "empty spaces" are replaced with water. Let us suppose that air eliminated is defined as $\dot{\varphi}_2^{(k)} \sim \varphi_2^{(k+1)} - \varphi_2^{(k)}$. The rate of change filling functions due to the air bubbles rise can be expressed as:

$$\begin{cases} \left(\dfrac{d\varphi_2^{(j)}}{dt}\right)_{el} = \alpha\,\varphi_2^{(j+1)} - \alpha\,\varphi_2^{(j)} \\ \left(\dfrac{d\varphi_1^{(j)}}{dt}\right)_{el} = -\dfrac{d\varphi_2^{(j)}}{dt} \end{cases} j=1,2,...,K-1,K, \quad (9)$$

where α is the air bubbles elimination proportionality coefficient, (s^{-1}), subscript *el* – elimination.

2.2. Sputtering and evaporation

Let us suppose that w_H is the frequency probability of the water droplets sputtered from the surface by the flux i_H. Usually, the water droplets can be sputtered only from monolayer covered with water. The rate of change filling functions due to sputtering can be expressed as:

$$\begin{cases} \left(\dfrac{d\varphi_1^{(j)}}{dt}\right)_{sp+ev} = \begin{cases} w_H \cdot \left(\varphi_1^{(j)}-\varphi_1^{(j-1)}\right), \; if \; \varphi_1^{(j)} \ge \varphi_1^{(j-1)} \\ 0, \; if \; \varphi_1^{(j)} < \varphi_1^{(j-1)} \end{cases} \\ \left(\dfrac{d\varphi_2^{(j)}}{dt}\right)_{sp+ev} = \dfrac{d\varphi_1^{(j)}}{dt} \end{cases} j=1,2,...K-1,K, \quad (10)$$

where $w_H = w_s + w_G = Y \cdot i_H + A\exp(-Q/k\cdot T)$, w_s is the freq-uency of probability of sputtering, w_G is the frequency of probability of evaporation, Y is the dimensionless coeff-icient of sputtering, k is the Boltzmann constant (J/K), T is the temperature (K), A is the evaporation coefficient, subscript $sp+ev$ denotes sputtering and evaporation.

2.3. Resorption

Sputtered water droplets can be resorbed back to the surface. Probabilities of resorbed water droplets sticking to the air or to the water are α_{ho} and α_{hh}, respectively. Following similar considerations used in deriving equation (10), the processes of resorption can be expressed as:

$$\begin{cases} \left(\dfrac{d\varphi_1^{(j)}}{dt}\right)_{resorb} = \begin{cases} \left(\varphi_1^{(j+1)} - \varphi_1^{(j)}\right)\cdot \chi_{HH} + \chi_{Hair}\varphi_2^{(j+1)}, & \text{if } \varphi_1^{(j+1)} \geq \varphi_1^{(j)} \\ \left(1 - \varphi_1^{(j-1)}\right)\cdot \chi_{Hair}, & \text{if } \varphi_1^{(j+1)} < \varphi_1^{(j)} \end{cases} \\ \left(\dfrac{d\varphi_2^{(j)}}{dt}\right)_{resorb} = \dfrac{d\varphi_1^{(j)}}{dt}, \qquad \alpha_{ho} \ll \alpha_{hh} \end{cases} \quad j=1,2,...K , \quad (11)$$

where $\chi_{HH} = \alpha_{hh} \cdot i_{Re}$, $\chi_{Hair} = \alpha_{ho} \cdot i_{Re}$, $i_{Re} = B \cdot i_{sput}$, $i_{sput} = w_H \cdot \left(\varphi_1^{(k)} - \varphi_1^{(k-1)}\right)$, α_{hh} is the water droplets sticking to the water probability, α_{ho} is the water droplets sticking to the air probability, i_{Re} is the flow of absorbed water droplets, B is the $(0 \leq B \leq 1)$ coefficient which defines the fraction of sputtered water returning to the surface. The first term in equation (11) describes the falling water droplet sticking to the water of K-th monolayer with the probability α_{hh}, the second term describes the falling water droplet sticking to the air with a probability α_{ho}.

3. RESULTS AND DISCUSSION

K monolayers are formed after air entrainment. These monolayers are filled with the air, air-water or water. Monolayer $K = 60$ was taken as a limitary monolayer. The last monolayer filled with the air and water was m-th and $m+1$ was filled only with water. For modeling according to equations (2) till (11) at time $t = 0$, such initial and boundary conditions were taken: $\varphi_2^{(K)}(0) = 1$, $\varphi_1^{(K)}(0) = 0$, when $K < 60$ and $\varphi_2^{(K)}(0) = 0$, $\varphi_1^{(K)}(0) = 1$, $\varphi_1^{(m)}(t) = \varphi_1^{(m+1)}(t)$ when $K \geq 60$. Solving equations $(2-11)$ initially was taken, that falling water flow in all monolayers is: $i_H = i_0 = $ const. Then for different Froude numbers monolayers filling with air decrease from one to zero (Fig. 1).

As can be seen from Fig. 1, the 60-th monolayer is the air - water interface monolayer. Filling of monolayers with the water is reciprocal process therefore it changes from zero to one.

For calculating the air and water concentrations in the monolayers according to equation (2) it was taken that the probability of the water droplets sticking to the water is $\alpha_{hh} = 0.95$, and for the air $-$ $\alpha_{ho} = 0.0000009$, sputtering coefficient $Y = 0.00095$.

Vertically falling water jet was used for stimulation of the air entrainment. During the experiment water flow fell into a vessel. The air temperature $T_{air} = 20\,°C$, the water temperature $T_w = 18\,°C$, the water density $\rho_w = 1000\ kg/m^3$,

water's surface tension $\sigma_w = 0,073\ N/m$, the pressure $P = 101.3\ kPa$. Detailed description of the experiment is presented in [28]. The experiment has shown that distribution of the concentration of the air entrained corresponds to the Gaussian distribution (Fig. 2).
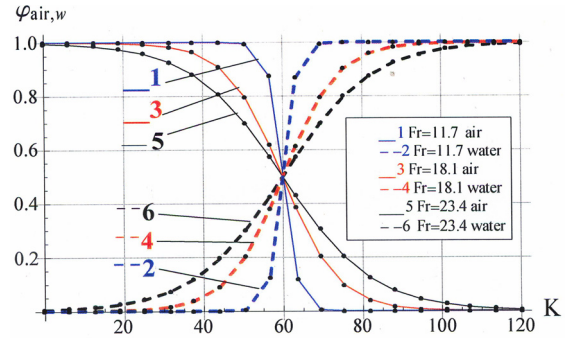

Fig. 1. Air and water distribution in monolayers for different Froude numbers $Fr_1 = 11.7, 18.1, 23.4$. Modeling was done according equations (2)–(11) taking that in all monolayers $i_H = i_0 = 0.095$

As can be seen from Fig. 2 the image representing the experiment consists of three parts. On the left side (Fig. 2, a) it is a real image of air bubbles and water droplets mixture. The central part of figure (Fig. 2, b) represents modified image of the air entrainment in the water. Computer program code analyzes the received images and presents data. For digital image processing the images library Python 2.7 was used [29]. The black digital image is the modified image of the air bubbles and the white image is of the water droplets. On the right side of the figure (Fig. 2, c) the change of concentration of the air entrained in depth and width is represented. In addition, the Figure 2, c, shows that air entrainment in deeper layers changes according to the Gaussian law. Therefore, for solving equations (4a) it was taken that falling water flow i_H is distributed in the monolayers to depth according to the Gaussian distribution.
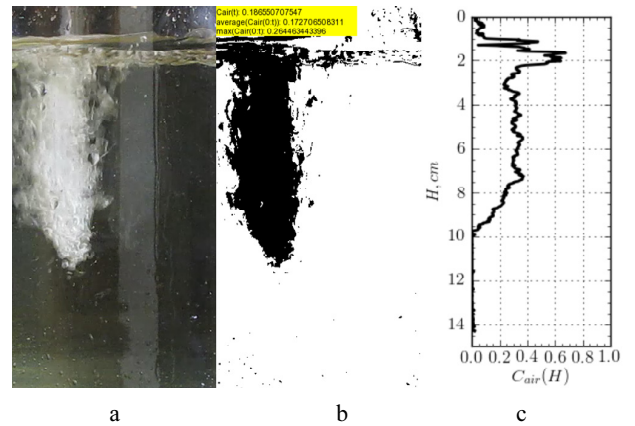

Fig. 2. Change of air entrainment; a – experimental real image, b – modified image, c – air concentration dependence on depth

Fig. 3 represents the change of dependence on the monolayers of filling with the air and water for different Froude numbers $Fr_1 = 11.7, 18.1, 23.4$. The average penetration depth R_p is calculated with empirical eq. (4b). As can be seen from Fig. 3 that the layer separating air and water is layer $K = 60$. Lines 1, 2, 3 show monolayers'

covered with water, and dashed lines 1, 2, 3 – with air (Fig. 3). Initially, the concentration of the air entrained increases till the maximum, then it decreases till reaches the air and water boundary and its value becomes zero. This process with water is reciprocal. As can be seen from inserted diagram (Fig. 3) the function φ_{max}^{air} slowly grows with increasing of the Froude number Fr_1. Also, maxima of concentrations of the air entrained slowly increases according to $\varphi_{max}^{air} \propto 0.3 \cdot \ln(Fr_1) - 0.58$. Thus, the inserted graph is a natural logarithm function.
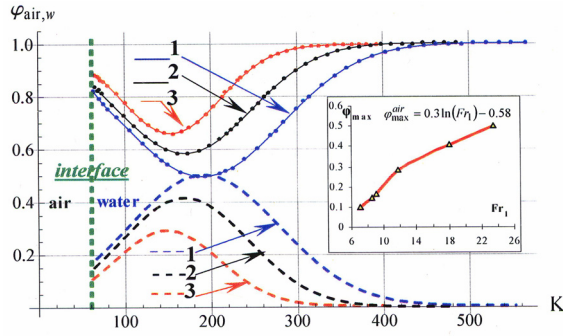

Fig. 3. Distribution of air and water in monolayers calculated different Froude numbers: 1 – $Fr_1 = 23.4$, 2 – $Fr_1 = 18.1$, 3 – $Fr_1 = 11.7$, when distribution is Gaussian. Modeling was done according equations (2). Inclusion shows maximum of air entrained dependence on Fr_1

Curve 3 (Fig. 3) corresponds Froude number $Fr_1 = 11.7$, maximum at $K = 165$, curve 2 – $Fr_1 = 18.1$ (maximum at $K = 195$), and curve 1 – $Fr_1 = 23.4$ (maximum at $K = 210$). Accordingly, with increasing Froude number the amount of the air entrained also increases. The average penetration depth of the air can be calculated according equation (4, b). This model was verified by the experiment taking $Fr_1 = 11.7$; 18.1; 23.4, nozzle diameter $d_0 = 0.004$ m, height of the falling flow $h = 0.25$ m, 0.5 m and 0.75 m. The results received from the experiment are presented in Fig. 4.
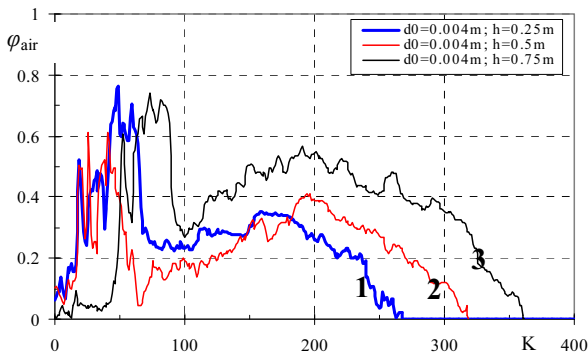

Fig. 4. Experimental data of air concentration distribution in monolayers, when 1 – $Fr_1 = 11.7$, 2 – $Fr_1 = 18.1$, 3 – $Fr_1 = 23.4$

As can be seen from Fig. 4, with Froude number increasing the maximal air entrainment in depth also increases and position of the maximum in the monolayer changes. Curve 1 – corresponds to the concentration of the air entrained, when $v_1 = 2.2$ m/s, $d_0 = 0.004$ m (diameter of nozzle), $d_1 = 0.0036$ m, $Fr_1 = 11.7$. Curve 2 – corresponds to concentration, when $v_1 = 3.1$ m/s, $d_0 = 0.004$ m,

$d_1 = 0.003$ m, $Fr_1 = 18.1$. Curve 3 – corresponds to the concentration, when $v_1 = 3.8$ m/s, $d_0 = 0.004$ m, $d_1 = 0.0027$ m, $Fr_1 = 23.41$ (Fig. 4). This experiment shows that with Froude number increasing air entrainment in depth changes i. e. increases, when velocity v_1 increases because $Fr_1 \sim v_1$. For modeling of the entrainment processes with equation (2) the influence of each parameter on the air and water concentration's changes should be considered separately. The influence of Froude number on the air entrainment was discussed above. Therefore, the influence of the falling water flow i_H (Fig. 5) should be also discussed.

Thus, for the solving equation we were taken that 60-th the layer is the air and water boundary layer it is worth to discuss the processes acting above monolayer 60-th. Change of the air concentration was signed with letter "a" and number (dashed lines in Fig. 5).
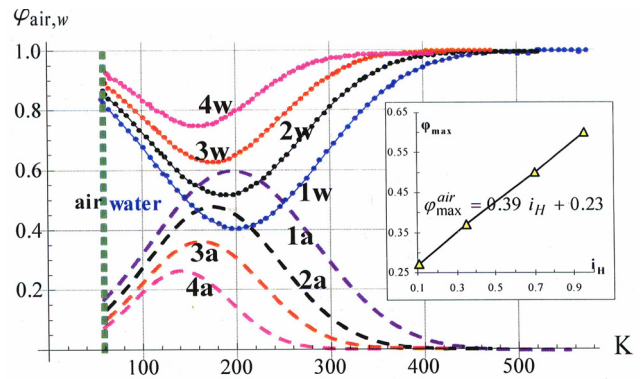

Fig. 5. Air and water concentrations distribution curves, when $Fr_1 = 30$. Dashed lines – concentrations of air, when 1a – $i_H = 0.95$; 2a – $i_H = 0.7$; 3a – $i_H = 0.35$; 4a – $i_H = 0.11$; Point lines – water concentrations, when 1w – $i_H = 0.95$; 2w – $i_H = 0.7$; 3w – $i_H = 0.35$; 4w – $i_H = 0.11$. Inclusion shows the maximum of air entrained dependence on falling water flow – i_H

For modeling with equation (2) was taken that $Fr_1 = 30$ and the falling flow changes from $i_H = 0.95$ to $i_H = 0.11$. The highest concentration of the air entrained was received when $i_H = 0.95$, $\varphi_{air} = 0.6$, $K = 200$ (Fig. 5, 1a).

As can be seen in inclusion (Fig. 5) the concentrations of maxima of the air entrained dependence on i_H is the linear function. Another important parameter is w_H. When $w_H = 0.0$, then also $w_s = 0.0$ and $w_G = 0.0$. In this case, there exist only the air entrainment and removal processes, the water droplets are not knocked out from the water surface. The modeling gives that the solutions of equations (10) and (11) are equal to zero. When during the falling flow $w_H \neq 0.0$ and $w_G = 0.0$, the concentration of the air entrained in the water increases with increasing w_H (Fig. 6). The graphic inserted (Fig. 6) shows the dependence of the maxima of the air entrained on parameter w_H. When the parameter w_H increases, then function of maxima of the air entrained is linear and can be described as: $\varphi_{max}^{air} \propto 0.58 \cdot w_H + 0.1$.

The parameter that must be evaluated is w_s. When $w_s = 0.0$, there is no water droplets sputtering, only the evaporation exists. Fig. 7 represents dependences of the air entrainment, when $T_{air} = 20$ ºC. As can be seen from Fig. 7,

when $w_s = 0.0$, the the curve of the concentration of the air entrained coincides with the curve of Fig. 8 when temperature $T = 20\,^{\circ}C$. With frequency of a probability of sputtering increasing concentration of the air entrained increases also. The inserted diagram (Fig. 7) shows that the dependence $\varphi_{\max}^{air} \propto 0.12 \cdot w_s + 0.25$ is linear, i.e. function φ_{max} increases linear with increasing of w_s.
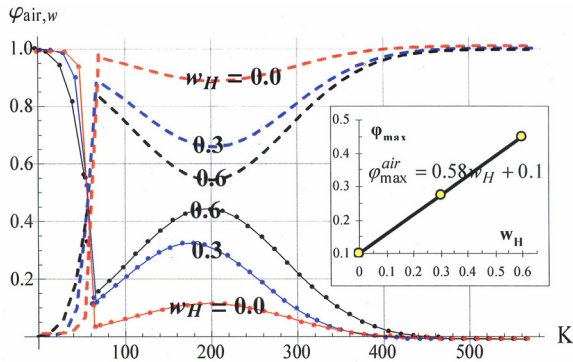

Fig. 6. Distribution concentrations of air entrained and water on monolayers. Dashed lines – water concentrations, when $w_H = 0.0$, $w_H = 0.3$ and $w_H = 0.6$. Doted lines – water concentrations, when $w_H = 0.0$, $w_H = 0.3$ and $w_H = 0.6$. In the inclusion is shown the air entrained maxima on w_H
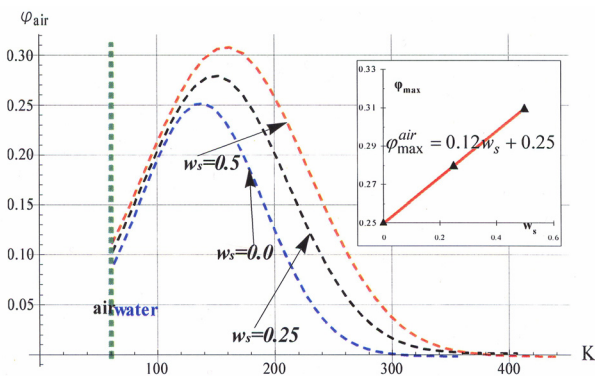

Fig. 7. Distribution of air concentration in monolayers, when $w_s = 0.0$, $w_s = 0.25$, $w_s = 0.5$. In the inclusion it is shown the air entrained maxima dependence on w_s
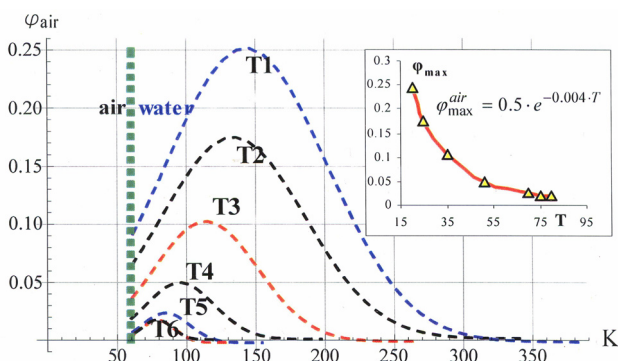

Fig. 8. Dependences of amount of air entrained in monolayers on temperature, when $T1 < T2 < T3 < T4 < T5 < T6$. Inclusion shows maximum of air entrained dependence on temperature

Among the parameters that influence distribution of concentration of air in monolayers the evaporation plays important role. The more water evaporates, the less air is entrained into the water (Fig. 8). Temperature has direct influence on the evaporation [30]. As can be seen from Fig. 8 the less temperature the more air is entrained into water. With growing temperature the evaporation increases and the amount of the air entrained into the water decreases. Completely different character has φ_{max} dependence on temperature (Fig. 8). This dependence shows that with temperature growing the maximum of the air entrained concentrations decreases in proportion with $\varphi_{\max} \propto 0.5 \cdot e^{-0.04T}$.

4. CONCLUSIONS

1. A new theoretical and experimental technique presented allowed determination of the air entrained concentration distribution below air-water interface. Theoretical and experimental results showed good coincidence.
2. Theoretical model gives that with increase of Froude number Fr_1, the maxima of the air entrained concentrations slowly increase according to a natural logarithm function.
3. Mathematical modeling showed that change (increase or decrease) of the falling water flow i_H causes linear change of the air entrained concentration's maxima according to linear function.
4. Sputtering of the water droplets depends on parameter w_H. The change of w_H leads to the liner change of maximum of the air entrained concentration according to linear function.
5. The air temperature influences processes of the evaporation and resorption. Theoretically was determined that increasing the air temperature, the maxima of the air entrained concentrations decrease according to a natural exponential function.

REFERENCES

1. **Zuev, B. K., Chudinova, V. V., Kovalenko, V. V., Yagov, V. V.** The Conditions of Formation of the Chemical Composition of the Sea Surface Microlayer and Techniques for Studying Organic Matter in It *Geochemistry International* 39 2001: pp. 702 – 710.
2. **Tsoukala, V. K., Moutzouris, C. I.** Gas Transfer under Breaking Waves: Experiments and Improved Vorticity-based Model *Annales Geographysicae* 26 2008: pp. 2131 – 2142.
3. **Deswal, S., Verma, D. V. S.** Air-Water Transfer with Multiple Plunging Jets *Water Quality Research Journal of Canada* 42 (4) 2007: pp. 295 – 302.
4. **Ichiyanagi, M., Tsutsui, I., Kakinuma, Y., Sato, Y., Hishida, K.** Three-dimensional Measurement of Gas Dissolution in Gas-liquid Microchannel Flow *International Journal of Heat and Mass Transfer* 55 2012: pp. 2872 – 2878.
5. **Li, W., Yang, K., Xia, M., Rao, J., Zhang, W.** Influence of Characteristics of Micro-bubble Clouds on Backscatter Lidar Signal *Optical Express* 17 (20) 2009: pp. 17772 – 17783.
6. **McGillis, W. R., Dacey, J. W. H., Ware, J. D., Ho, D. T., Bent, J. T., Asher, W. E., Zappa, C. J., Raymond, P. A., Wanninkhof, R., Komori, S.** Air-water Flux Reconciliation between the Atmospheric CO_2 Profile and Mass Balance Techniques C. S. Garbe, R. A. Handler,

B. Jahne (editors)   In Transport at the Air-sea Interface: Measurements, Models and Parameterizations. Springer Verlag 2007: pp. 1 – 15.
http://dx.doi.org/10.1007/978-3-540-36906-6_13

7. **Alves, S. S., Maia, C. I., Vasconcelos, J. M. T.** Gas-liquid Mass Transfer Coefficient in Stirred Tanks Interpreted through Bubble Contamination Kinetics   *Chemical Engineering and Processing*   43   2004: pp. 823 – 830.
http://dx.doi.org/10.1016/S0255-2701(03)00100-4

8. **Baawain, M. S., El-Din, M. G., Smith, D. W.**   Characterizing Two Inclined Circular Water Jets Plunging into an Aeration Tank   *International Journal of Multiphase Flow*   40   2012: pp. 158 – 165.

9. **Mölder, E., Tenno, T., Tenno, T.** Reseach of Oxygen Mass Transfer through the Air-water Surface at Low Bulk Concentrations of Surfactants   *Proceedings of Estonian Academy of Sciences*   58   2009: pp. 132 – 136.

10. **Donelan, M., Wanninkhof, R.** Gas Transfer at Water Surfaces-components and Issues   *Geophysical Monograph*   127   *Gas transfer at Water Surfaces*   2002: pp. 1 – 10.

11. **Luu, Li-Hua, Forterre, Y.** Drop Impact of Yield-stress Fluids   *Journal of Fluid Mechanics*   632   2009: pp. 301 – 327.

12. **Vaidelienė, A., Galdikas, A., Vaidelys, V.**   Water Turbulence after Hydropower's Plants Influence on Gas Diffusion Processes   *International Scientific Conference Energy Efficiency and Agricultural Engineering (EE&AE'2009): Proceedings of the Union of Scientists, Rousse Fourth Conference, Bulgaria, October 1 – 3, 2009.* Bulgaria: Association of Agricultural Engineering in Southeastern Europe, 2009: pp. 883 – 889.

13. **Kowal, J. J, Turchan, A., Heller, K., Brenizer, J., Mench, M. M.** Liquid Water Storage, Distribution, and Removal from Diffusion Media inPEFCS   *Journal of the Electrochemical Society*   153 (10)   2006: p. 971.
http://dx.doi.org/10.1149/1.2258049

14. **Yeghiazarian, L., Samorodnitsky, G., Montemagno, C. D.** A Poisson Random Field Model of Pathogen Transport in Surface Water   *Water Resources Research*   45   2009: pp. W11415: 1 – 10.

15. **Baawain, M. S, El-Din, M.G., Smith, D.W.** Characterizing Two Inclined Circular Water Jets Plunging into an Aeration Tank   *International Journal of Multiphase Flow*   40   2012: pp. 158 – 165.

16. **Vaidelienė, A., Mihailov, N.** Influence on the River Self-purification   *Environmental Engineering: 7th International Conference, Vilnius Gediminas Technical University, May 22-23, 2008.* Vilnius: VGTU Press "Technika", Vol II. 2008: pp. 748 – 757.

17. **Toombes, L., Chanson, H.** Interfacial Aeration and Bubble Count Rate Distributions in a Supercritical Flow Past a Backward-facing Step   *International Journal of Multiphase Flow*   34   2008: pp. 427 – 436.

18. **Hoqua, A., Aoki, S.** Air Entrainment and Associated Energy Dissipation in Steady and Unsteady Plunging Jets at Free Surface   *Applied Ocean Research*   30   2008: pp. 37 – 45.

19. **Karwa, N., Schmidt, L., Stephan, P.** Hydrodynamics of Quenching with Impinging Free-surface Jet   *International Journal of Heat and Mass Transfer*   55   2012: pp. 3677 – 3685.
http://dx.doi.org/10.1016/j.ijheatmasstransfer.2012.02.035

20. **Miliauskas, G., Šinkūnas, S., Miliauskas, G.** Evaporation and Condensing Augmentation of Water Droplets in Flue Gas   *International Journal of Heat and Mass Transfer*   53   2010: pp. 1220 – 1230.

21. **Miliauskas, G., Sabanas, V.** Interaction of Transfer Processes during Unsteady Evaporation of Water Droplets   *International Journal of Heat and Mass Transfer*   49   2006: pp. 785 – 798.

22. **Miliauskas, G.** Regularities of Unsteady Radiative-conductive Heat Transfer in Evaporating Semitransparent Liquid Droplets   *International Journal of Heat and Mass Transfer*   44   2001: pp. 785 – 798.

23. **Miliauskas, G., Sabanas, V., Bankauskas, R., Miliauskas, G., Sankauskaite, V.** The Peculiarities of Sprayed Liquid's Thermal State Change, as Droplets Are Heated by Conduction   *International Journal of Heat and Mass Transfer*   51   2008: pp. 4145 – 4160.

24. **Miliauskas, G., Garmus, V.** The Peculiarities of Hot Liquid Droplets Heating and Evaporation   *International Journal of Heat and Mass Transfer*   52   2009: pp. 3726 – 3737.
http://dx.doi.org/10.1016/j.ijheatmasstransfer.2009.03.001

25. **Deswal, S.** Modeling Oxygen-transfer by Multiple Pluging Jets using Support Vector Machines and Gaussian Process Regression Techniqus   *Word Academy of Science, Engieering and Technology*   73   2011:pp. 28 – 33.

26. **Chanson, H.** Convective Transport of Air Bubbles in Strong Hydraulic Jumps   *International Journal of Multiphase Flow*   36   2010: pp. 798 – 814.
http://dx.doi.org/10.1016/j.ijmultiphaseflow.2010.05.006

27. **Sande, van de E., Smith, J. M.** Mass Transfer from Plunging Water Jets   *Chemical Engineering Journal*   10   1975: pp. 225 – 233.

28. **Vaidelienė, A., Tervydis, P.** Measurement of Air Bubbles Concentration in the Water by Means of Digital Image Processing   *Electronics and Electrical Engineering*   4   2013: pp. 77 – 80.

29. **Valantinas, J., Kančelkis, D.** Speeding-up Image Encoding Times in the SPIHT   *Algoritm Information Technology and Control*   40 (1)   2011: pp. 7 – 12.

30. **Miliauskas, G., Šinkūnas, S, Norvaišienė, K., Šinkūnas, K.** Initial Water Temperature Influence on the Thermal State of Evaporating Droplets   *Mechanika*   19 (2)   2013: pp. 135 – 142.